Particle Accelerators
1980 Vol.10 pp.223-234
0031-2460/80/1003-0223$06.50/0

THE DESIGN AND PERFORMANCE OF A LONG-PULSE HIGH-CURRENT LINEAR INDUCTION ACCELERATOR AT THE NATIONAL BUREAU OF STANDARDS*

JAMES E. LEISS,† NEIL J. NORRIS‡ and MARK A. WILSON

Center for Radiation Research, National Bureau of Standards, Washington, D.C. 20234 USA

(Received April 14, 1980)

A prototype module of a unique long-pulse, low-cost, high-energy, high-current induction linear accelerator has been designed, constructed and tested at the National Bureau of Standards (NBS). Tests prove that such modules are capable of accelerating several kiloamperes at a voltage gradient of better than 0.25 MeV per meter. Combined with a high-current injector, the prototype module has accelerated a 1-kA, 2-μsec (FWHM) electron beam pulse to over 0.8 MeV with a computed energy spread of less than 3% (FWHM).

1. INTRODUCTION

A program was begun in 1970 to study the theoretical and technical feasibility of the induction linear accelerator as an electron beam generator for applications requiring high energy, long pulse, and high beam current. Induction linear accelerators had already been developed at the Lawrence Radiation Laboratory to produce electron beams of several hundred amperes in pulses of 40 nsec[1] and 300 nsec[2] in length at energies up to 4 MeV and 5 MeV, but it was considered that the techniques developed for these induction accelerators would not be practical for accelerating longer pulses to much higher energies. Therefore, the effort at NBS was directed toward extending the technology to less-costly, more-abundant magnetic materials to be used at maximum efficiency. The accelerator modules were designed using new material, to attain high voltages for long pulse lengths at a minimum cost, and to minimize the length and complexity of a high-energy accelerator. In order to maximize the current that could be transmitted stably through an extended accelerator, a beam-transport computer code was developed[3] that included self-fields, wall effects and residual-gas effects, in addition to external magnetic focusing elements. In concert with the beam-transport studies, a program was undertaken to discover and suppress modes of high-current beam breakup in the accelerator.[4]

One of the goals accomplished during the NBS program was to build a low-energy prototype accelerator based on the results of the investigations into materials, techniques and fabrication procedures, thereby demonstrating engineering feasibility and cost savings.

Following a brief treatment of the principle of induction acceleration and a description of the innovations resulting from scale-model design studies, the remainder of the present paper will deal with the design, construction and performance of the prototype built at NBS.

2. THE PRINCIPLE OF LINEAR INDUCTION ACCELERATION

The principle of linear acceleration by magnetic induction is demonstrated in the schematic in Fig. 1. A beam of charged particles passes through a toroidal core of ferromagnetic material at the same time that a change in flux in the core is produced by a voltage pulse applied to a driving loop. A voltage appears across a gap in a second loop during the flux change according to the expression

$$V_{\text{gap}} = \oint \mathbf{E}\cdot d\mathbf{l} = -\int \frac{d\mathbf{B}}{dt}\cdot d\mathbf{s}. \qquad (1)$$

* Work supported in part by the Office of Naval Research

† Present Address: Office of Energy Research, Mail Station J-309, Department of Energy, Washington, D.C. 20545

‡ Present Address: E.G. & G., 130 Robin Hill Road, Goleta, CA 93017

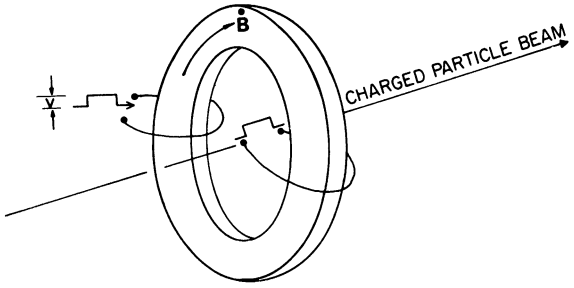

FIGURE 1 Schematic showing the principle of induction acceleration.

The particles that thread the core during the pulse are accelerated in the field across the gap in the second loop and complete the line integral in Eq. (1). The surface integral is taken over the cross section of the core. The accelerating voltage will be maintained in the gap until either the driving pulse terminates or the toroidal core material reaches magnetic saturation. At the time τ of core saturation, the drive current increases, the gap voltage decreases because of the generator impedance, and dB/dt decreases suddenly. If dB/dt is assumed constant over the core cross-sectional area, A, then at the time of core saturation, Eq. (1) yields

$$V_g\tau = A\Delta B,$$

where ΔB is the total change in the magnetic flux density.

To maximize the time before saturation, the total change in magnetic field in the core should be maximum. The hysteresis loop for a typical ferromagnetic material, Fig. 2, illustrates the added total flux change made available by driving the core to reverse field saturation before an accelerating pulse. This is usually accomplished by applying a long low-voltage pulse of opposite polarity to reset the core in a reversed field state.

Since a voltage is induced only in circuits threading the core of an induction accelerator module, the voltages of a sequence of modules successively add to the energy of an axial particle beam. This concept is demonstrated in Fig. 3, which shows the beam being accelerated across each gap in a succession of single-core modules while the beam tube is grounded at both ends of each module. Beam energy in induction linacs is therefore limited only by practical accelerator length.

The induction accelerator is inherently a low-impedance device, because the accelerating voltage is developed by a single turn that surrounds the toroidal magnetic core. It is particularly suited to high-current accelerator applications where the output of the drive-pulse circuitry can be efficiently matched to beam currents of several kiloamperes.

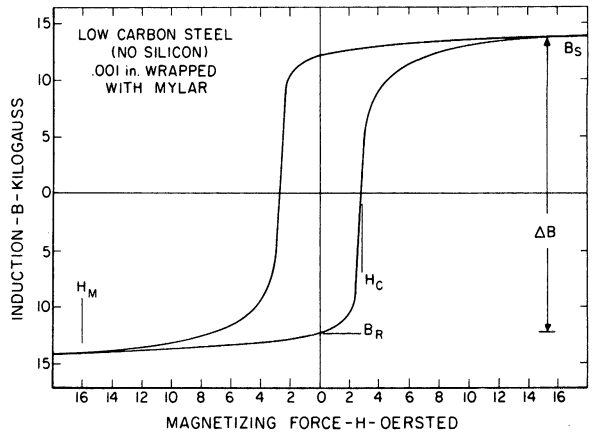

FIGURE 2 Magnetic hysteresis loop for a small mild steel foil toroidal core.

Eddy-current losses may be minimized by winding the toroidal core of thin laminations. Kuenning[5] and Winter[6] have employed a saturation wave analysis to treat the behavior of laminated iron cores undergoing rapid magnetic excitation. Their work resulted in semiempirical formulas that describe the saturation of the iron and predicted the eddy currents in the Lawrence Livermore Laboratory's[2] accelerator cores reasonably well. In these formulas, the product of the voltage V developed in a circuit around the

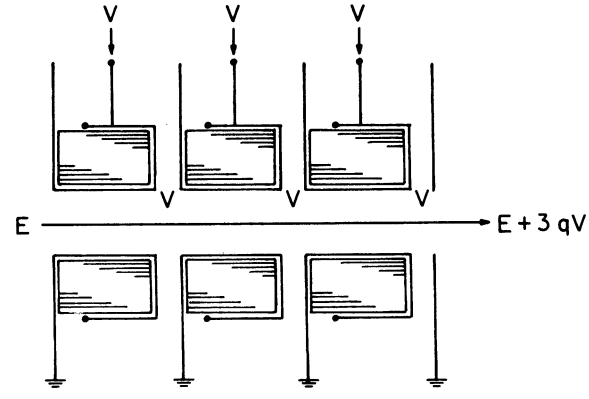

FIGURE 3 Schematic cross section of several single-core units in tandem to show sequential energy increase. q is the charge state of the beam particles.

core and the time τ to saturation of the innermost foil wrap is given by

$$V\tau = \Delta BAS \frac{2}{1 + \sqrt{a/b}}. \quad (2)$$

Prior to inner wrap saturation the eddy current in the core increases linearly with time as

$$i(t) = \frac{\pi}{2}\left(\frac{V}{AS}\right)^2 \frac{bd^2t}{\Delta B\rho}\left(\frac{1 + \sqrt{a/b}}{2}\right)^2, \; t \leq \tau: \quad (3)$$

The core current just prior to saturation is obtained by combining Eq. (2) with Eq. (3) at $t = \tau$ to find

$$\frac{i(\tau)}{V} = \frac{\pi}{2}\frac{b}{AS}\frac{d^2}{\rho}\left(\frac{1 + \sqrt{a/b}}{2}\right), \quad (4)$$

where ΔB is the available flux-density change (Tesla), A is the $(a - b)W$ cross-section area of core (meter^2), a is the outer radius of core (meters), b is the inner radius of core (meters), W is the width of core (meters), d is the foil thickness (meters), ρ is the foil resistivity (ohm-meters), and S is the packing factor (fraction of $a - b$ that is iron).

These expressions are used to relate the core geometry and the electric and magnetic properties of core material to the design of induction accelerator elements. For example, by proper selection of core material and lamination thickness, according to the term d^2/ρ in Eq. (3), the eddy current is minimized, thereby improving the efficiency of energy transfer to the beam. Economic factors will also contribute to the selection of core material.

3. RESULTS OF SCALE-MODEL STUDIES

In order to achieve a nearly optimal energy gain per module and to utilize the core material efficiently, as well as to establish a design leading to an accelerator that would be simple and reliable to operate, small single cores and scale-model components up to one-fourth prototype size were built and tested.

Single cores were used for studies of magnetic materials and fabrication techniques. Ferrite, used in the Lawrence Berkeley Laboratory's ERA injector,[1] saturates at too low a magnetic field for practical long-pulse application. Table I lists the pertinent properties of three more-likely candidate materials. Nickel-iron alloy tape has the lowest coercive force H_c and therefore the lowest loss due to magnetizing currents. It can be rolled into thin foil for low eddy-current losses and was used in the Lawrence Livermore Laboratory's Astron injector.[2] It would, however, be prohibitively expensive and difficult to acquire in the large quantities needed for a long-pulse high-energy accelerator. Therefore, tape-wound cores of silicon-iron alloy and of plain mild steel were tested. Large quantities of iron with 3.25% silicon are produced for the transformer industry and could be made available in foil thin enough (0.05 mm) to keep eddy-current losses to an acceptable level. But large quantities of 0.025-mm (0.001 in.) mild-steel foil could be obtained at one-fourth the cost per finished core, which leads to a considerable cost saving for a large accelerator. A comparison of H_c for mild steel and silicon-iron indicates that higher magnetizing currents will be required for the mild steel, but from the values of resistivity ρ given in Table I, it is seen that the use of mild steel foil of half the thickness d of silicon-iron would result in eddy currents of comparable magnitude in both materials, since, according to Eq. (3), eddy currents vary as d^2/ρ. From the table the available flux-density change ΔB is only about 10% less in mild steel than in silicon-iron. The results of small core tests were in reasonable agreement with these numbers; therefore, the less-expensive material was chosen for the prototype cores.

In order to achieve a large energy gain per accelerating module, high voltages must be sustained across the tape-wound iron cores. Experiments showed that, by winding the iron foil together with 0.0063 mm (0.00025 in.) mylar sheet as a positive interlaminar insulation, volt-

TABLE I

Magnetic and Electrical Properties of Candidate Core Materials, 0.002 Inch Foil, Annealed

Material	$H_c(O_E)$*	$H_M(O_E)$*	B_S(kG)*	B_R(kG)*	$\rho(\mu\Omega\text{-cm})$
[a]Nickel-Iron	0.1	16.	15.6	14.6	45
[b]Silicon-Iron	0.6	16.	16.5	14.6	50
[c]Mild Steel	2.5	16.	14.6	13.9	12.75

[a] From *Electrical Materials Handbook,* Allegheny Ludlum Steel Corporation. Pittsburgh, 22, Pa (1961), pp. VII/50, VII/52.
[b] **Op. cit.,** pp. IX/2, IX/25.
[c] U.S. Steel Company, private communication.
* See Fig. 2.

age breakdown could be prevented. A liquid polyester resin was applied during the winding process and then cured to yield rigid, self-supporting cores. The ability of individual cores to be self-supporting simplified the design of full-scale modules.

The use of mylar and polyester as an interlaminar insulation has the disadvantage that the completed core assembly cannot be annealed, as is often done with toroidal transformer cores. The strains and grain distortions caused by handling and winding under tension increase the magnetization losses and reduce the usable flux-density swing ΔB of the completed core compared with the value for annealed laminations. The use of this positive interlaminar insulation in nickel-iron cores is not practical, because the excellent magnetic properties of nickel-iron are considerably reduced by handling. Although applying this positive insulation to silicon-iron or mild steel after annealing does affect their magnetic properties to some extent, the degradation in performance is not so severe as in nickel-iron.

For long pulse and high energy gain, a large cross section of magnetic material is required. To attain this cross section while keeping to a reasonable axial length of the accelerator requires a large ratio of outer to inner radius of the accelerator cores. In addition, maximum utilization of the magnetic material occurs if the entire core saturates at the same time, but the material at the inner radius of the core saturates first, after which time the core loading increases rapidly. For a core with a large ratio of outer to inner radius, as in Fig. 4a, much of the core is only partially magnetized before the inner material is saturated. This problem is reduced by segmenting the core so that the inner and outer radii of each core segment are made more nearly equal, as in Fig. 4b. The practicality of this concept was verified in studies using scale-model segmented core sets. By driving all radial segments of each core in parallel and choosing the segment radial dimensions according to Eq. (2) so that all segments of a core saturate at the same time, maximum use is made of the magnetic material. For the full-scale cores, this method increases the iron utilization from nearly fifty percent to about ninety percent.

The above innovation has led to another benefit, which is of particular importance in achieving a high energy gain per module. Since the secondary loop containing the accelerator gap encircles all the core segments, as in Fig. 4b, the accelerating voltage is the sum of the individual

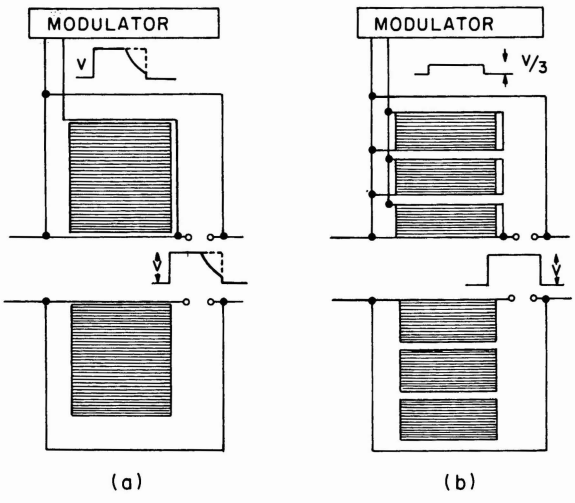

FIGURE 4 Schematic cross section of an induction accelerator unit showing: (a) a single core with a large ratio of outer to inner radius, (b) radial core segments with nearly the same total cross-section area as (a), but with a smaller ratio of outer to inner radius in each segment. In (b), magnetic saturation occurs later in the pulse and more uniformly throughout the core material. Note that, for 3 core segments, the modulator drive voltage is only ⅓ the accelerating voltage.

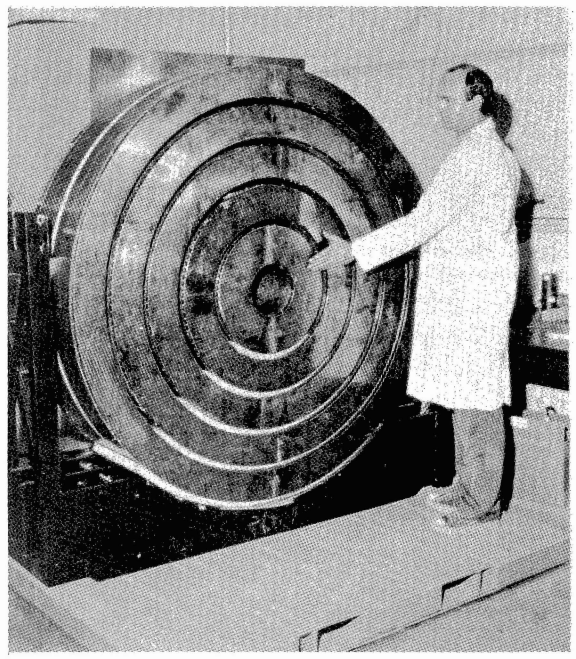

FIGURE 5 Photograph of the assembled five-core set, showing copper sheet wrapped onto each core segment as the primary turn.

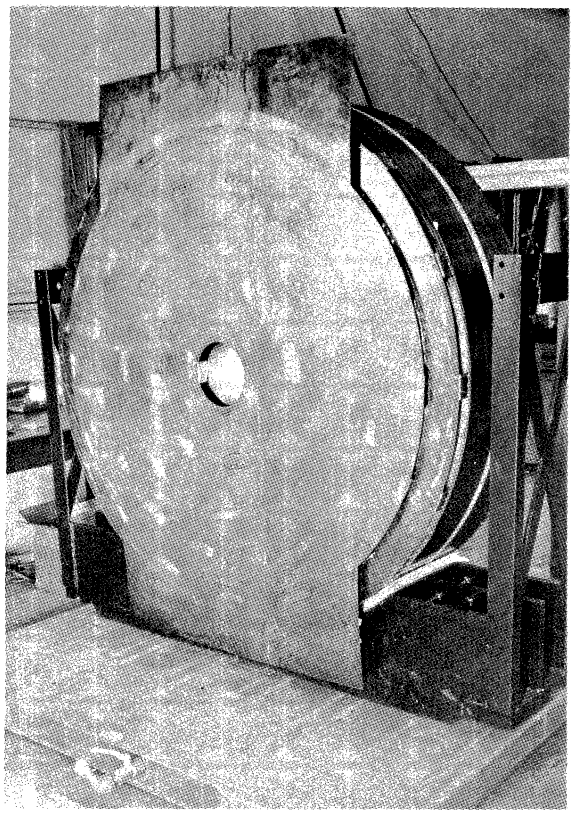

FIGURE 6 Photograph of the reverse side of the five-core set, showing the low-inductance drive planes installed on the core segments.

segment voltages. This proves to be an efficient step-up transformer whose voltage ratio is equal to the number of segments. Voltage step-up is advantageous because the operating voltage of the modulator components is reduced. This reduction in operating voltage permits less-expensive, more-reliable pulse-forming networks to be used in the accelerator. The step-up ratio appears to be limited only by the correspondingly low impedance that must be driven by the modulator, which is usually a pulse-forming network (PFN) of inductances and capacitors. The load current, which is driven by the PFN, is a parallel combination of the beam current (assumed constant during the pulse) and core currents, which increase during the pulse.

For optimum energy resolution, the accelerating voltage pulse shape should be as flat as possible. Although the linearly increasing eddy currents in the core [refer to Eq. (2)] can be offset by tapering the impedance of the pulse line, the pulse-line taper will produce a flat accelerating voltage for only one beam current. Scale-model tests confirmed that a compensating network consisting of a series resistor and capacitor in parallel with the cores can be made to offset the increase in core eddy current sufficiently so that the total impedance of the core plus RC compensator would be nearly constant. In this way the drive voltage delivered by a constant-impedance pulse line would remain constant, independent of beam load.

4. THE PROTOTYPE ACCELERATOR MODULE

The prototype accelerator module was designed on the basis of the scale-model results according to Eqs. (2–4). Figure 5 is a photograph of an assembled set of cores. The inner and outer wrap of each core segment is a 0.51-mm copper sheet. These sheets are connected together to form a compact conducting turn around each segment. These turns are connected in parallel by way of two copper sheets as shown in Fig. 6. The large parallel drive and ground planes, coupled to each closely wrapped primary turn, form a compact

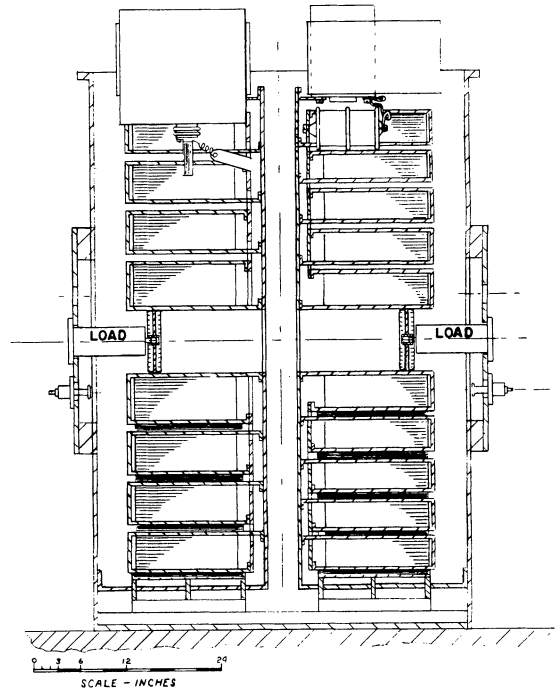

FIGURE 7 Schematic cross section of the assembled prototype module. The hatched area around each core segment represents the copper sheet.

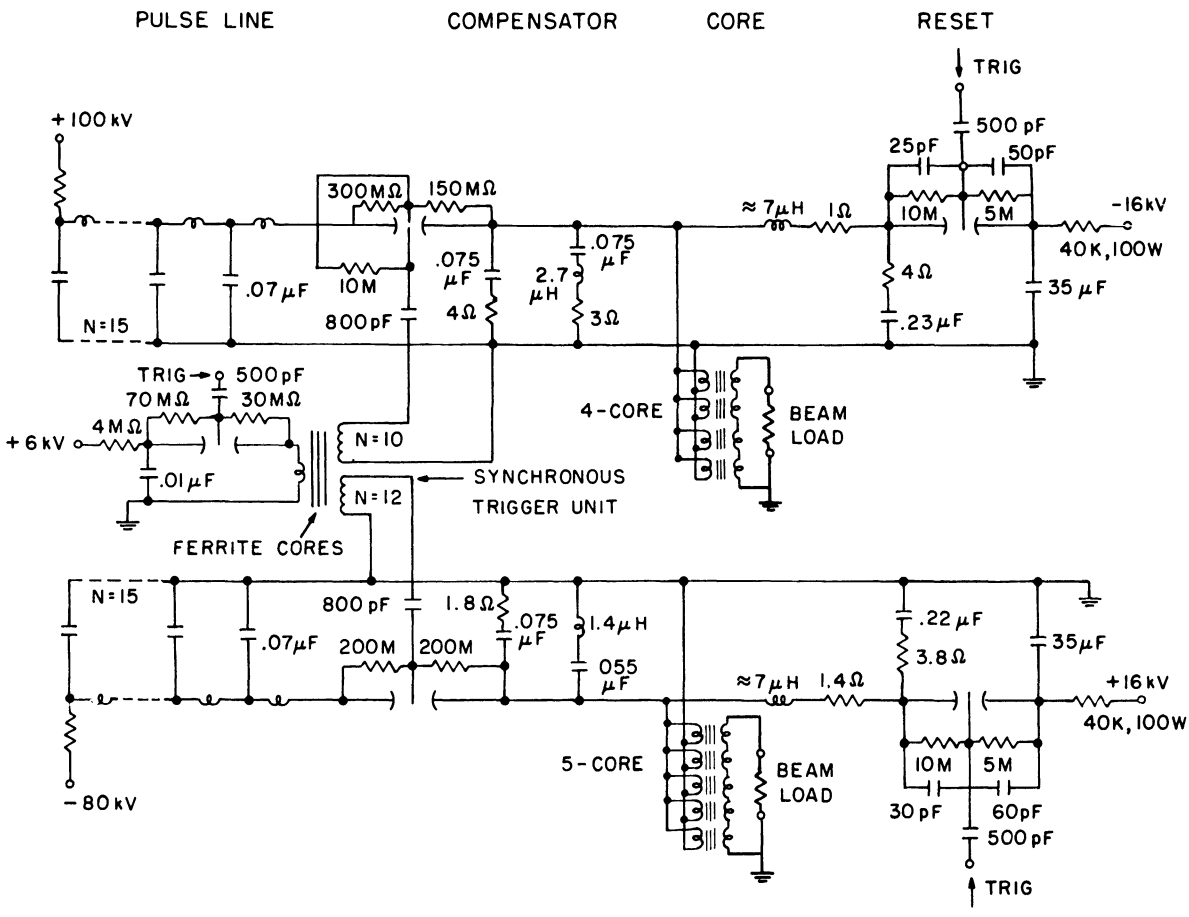

FIGURE 8 The electric circuit of the prototype module.

low-inductance drive system with very high current capability.

Figure 7 is a schematic cross section of the assembled prototype module showing the primary-turn configuration and drive connections in more detail. The prototype module consists of two nested core sets, with modulators, mounted in an oil-filled tank. One of the core sets is composed of five radial segments while the other is of four radial segments in order to permit performance comparisons. Each set weighs approximately 4100 kg and is designed to sustain 200 kV for 2 μsec before saturation. Although the module was designed to be pulsed at a rate of one pulse per second without thermal load problems, the system is presently limited to one pulse per minute by the charging rate of the power supplies.

The energy to drive a core set is stored in a multi-section lumped-constant pulse line that is discharged through a spark-gap switch. The modulator, composed of pulse line, switch and compensator circuit, is mounted over the core set for close coupling. Space was also made available in the modulator for the reset circuit. A schematic of thc electrical circuit of the prototype module is shown in Fig. 8. Typical values of the circuit parameters are included in the figure. The series inductors of the pulse line were adjusted so that the characteristic output impedance was 1.4 ohms for the four-core pulse line and 1.29 ohms for the five-core pulse line. The 15 capacitors in each line provide sufficient pulse length to drive the core sets into saturation when discharged into a matched load after being charged to their rated voltage of 100 kV. The trigger circuit, also shown schematically in Fig. 8, discharges both pulse lines synchronously to within 50 nsec.

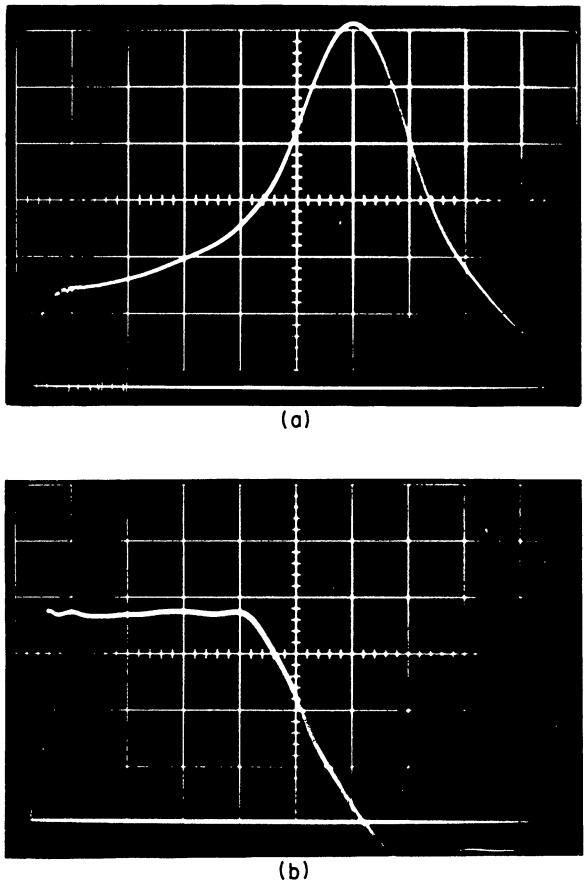

FIGURE 9 Oscilloscope traces of (a) core current and (b) drive voltage pulses of the five-core set near half voltage. Horizontal scale: 1.0 μsec/large division. Vertical scale: (a) 5.5 kA/large division, (b) 5.0 kV/large division.

4.1 Preliminary Prototype Tests

Each core set was pulse tested with the accelerating gap replaced with a variable-resistance salt-water load (shown in Fig. 7) for current and voltage performance tests. The secondary-gap voltage was determined from a capacitive pick-up which was calibrated using a high-voltage probe. This probe was, in turn, checked against an electrostatic voltmeter. Coaxial shunts, calibrated against a precision ammeter, were used for current monitoring. Measured core currents consist of eddy currents plus magnetizing currents.

Figure 9a shows the sum of core currents of the five-core set at a drive voltage of 18.6 kV. The initial step in the core current pulse appears to correspond to the magnetizing current required to overcome the coercive force of the core material. Figure 9b shows the drive-voltage pulse. Note that the voltage remains essentially constant while the core current is increasing. This demonstrates the effectiveness of the compensator circuit in maintaining a constant total load. It was found that the addition of inductance to

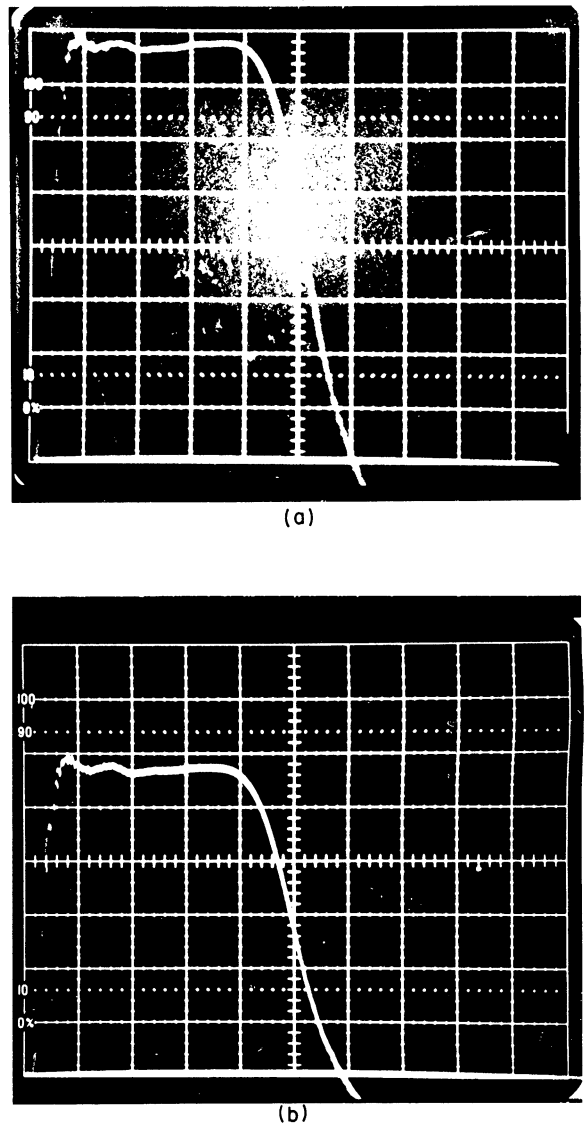

FIGURE 10 Oscilloscope trace of (a) gap voltage and (b) gap current of the five-core set at full voltage. Horizontal scale: 0.5 μsec/large division. Vertical scale: (a) 26 kV/large division, (b) 440 A/large division.

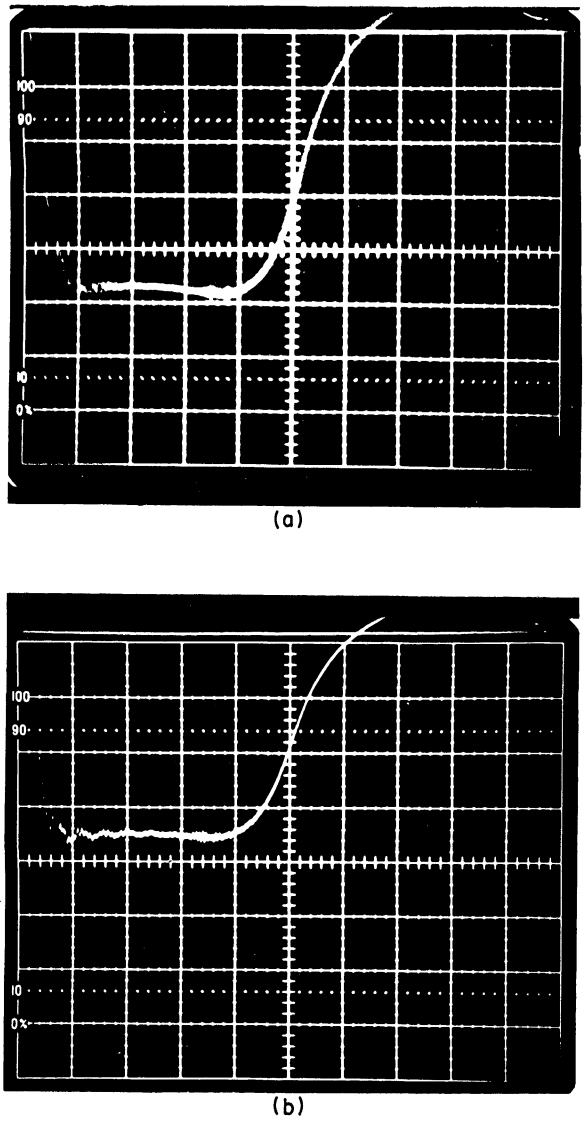

FIGURE 11 Oscilloscope trace of (a) gap voltage and (b) gap current of the four-core set near full voltage. Horizontal scale: 0.5 μsec/large division. Vertical scale: (a) 41 kV/large division, (b) 880 A/large division.

the compensator network provided for constant total impedance more efficiently (higher total impedance) and for a longer period before core saturation loaded down the pulse line. Typical values of the compensator-circuit components for full drive voltage are given in Fig. 8.

Following the development of effective pulse-shaping circuitry, both sets of cores were pulse-tested to the design output voltage of 200 kV. The performance of the five-core set at 200 kV is shown in Figs. 10a and 10b. The load current across the output was 2.5 kA (Fig. 10b). A charging voltage of 84 kV was required to maintain this load at 200 kV. Since the voltage step-up is five to one, the drive voltage is 40 kV for an output voltage of 200 kV. Under these conditions, the transformed output load together with the core and compensator loads nearly match the characteristic impedance of the pulse line. (When the load matches the characteristic impedance of the pulse line, the discharge pulse voltage equals one-half the charging voltage.) Figures 11a and 11b show the output voltage and current from the four-core set under matched conditions at design voltage. The pulse line must be charged to 100 kV to achieve 200 kV output since the voltage step-up is only four to one. The matching output current load of 3.25 kA (Fig. 11b) is higher than for the five-core set because the transformed impedance is higher in the case of four cores.

To study the effect of high voltage stress, the five-core set was repeatedly pulse tested up to 247 kV output voltage under a reduced output load. No voltage breakdowns were observed during the 23% increase over the design voltage.

Based upon the small-core tests, the prototype module core sets were designed to sustain an output voltage of 200 kV for 2.0 μsec. However, design voltage was produced for only 1.6 μsec, corresponding to a 20% reduction in usable flux swing in the prototype cores. In addition, the core-current loading calculated from the performance tests of the mild-steel prototype cores represents nearly two-thirds of the total load under matching conditions. This level of observed currents (the sum of eddy currents plus magnetizing currents) appears higher in the prototype cores than expected from the small-core tests. This increase is most probably due to stresses incurred during the core-winding process, which seem to have affected the magnetic properties of the steel foil. It is believed that both the usable flux swing and the efficiency of full size mild steel cores can be improved with future development work that includes a study of the effects of preparation and handling on the magnetic properties of the core material.

4.2 Beam Tests

In order to establish the performance of the prototype module as an induction accelerator, a high-current electron-beam injector was con-

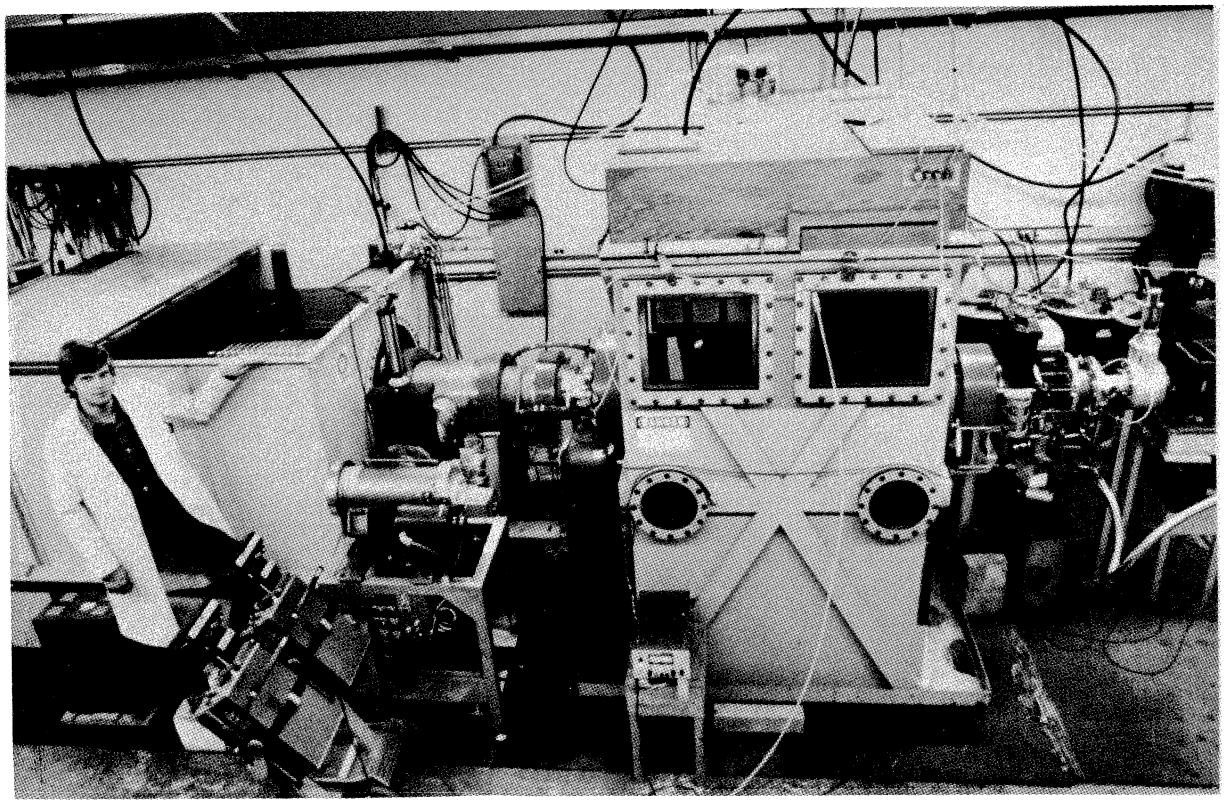

FIGURE 12 Photograph of the three-stage prototype accelerator. The injector tank is on the left. The accelerator module is at middle right.

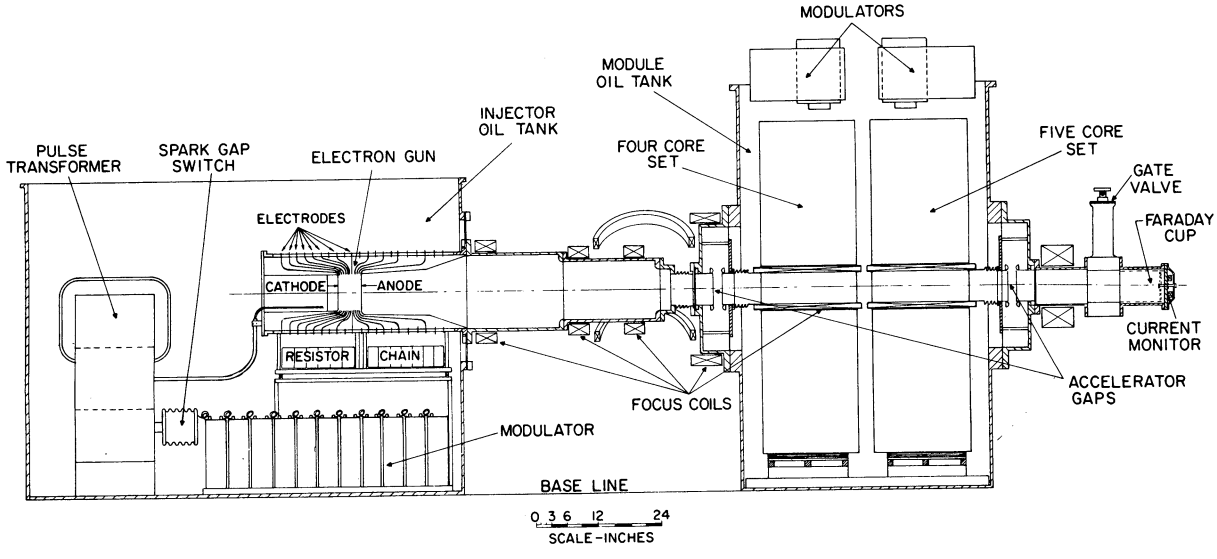

FIGURE 13 Schematic cross section of the three-stage prototype accelerator.

structed and coupled to the module to form the three-stage accelerator shown pictorially in Fig. 12 and in schematic cross section in Fig. 13.

In the injector, contained in an oil-filled tank, a pulse line discharges through a spark gap into the single primary turn of a pulse transformer with a twelve-turn secondary. The core of the transformer is similar to one of the cores of the induction module. The output of the transformer drives an electron gun containing a thermionic cathode with a 16.5-cm diameter active surface. Heater power of up to 3.5 kW is delivered to the cathode filament by leads wound coaxial with the secondary winding of the pulse transformer. This coaxial winding technique proved to be a simple solution to the problem of isolating the filament power source from pulsed high voltage. Electrons from the cathode are accelerated in the gun through a series of 22 annular electrodes (shown schematically in Fig. 13) spaced by ceramic insulator rings, which are silver-brazed to the electrodes to form the vacuum envelope. The voltage on the electrodes is distributed by a low-inductance resistor chain. The last electrode forms a grounded anode and has a 95%-transmission tungsten screen stretched over the 16.5-cm diameter aperture. The spacing between electrodes is such as to provide a focusing electric field in the anode-cathode gap region. The injector has accelerated 1.2 kA of electrons to 500 keV for 2.0 μsec (FWHM), but the usual procedure is to operate the gun at about 400 keV and 0.85 kA to avoid high-voltage breakdown. Figure 14 shows typical injector-voltage and cathode-current pulses.

The prototype induction accelerator module is shown schematically in Fig. 13, connected to the output of the injector, with the four-core and five-core accelerating gaps and vacuum pipe installed. The series of focusing solenoids shown in the figure have been designed[3] to maximize high-current beam transmission by providing focusing fields along the full length of the accelerator. Up to 95% of the beam passing through the injector anode has been delivered to the output of the prototype module, as measured by a Faraday cup and current transformer. Figure 15 shows the beam-current pulse at the accelerator exit.

Figure 16 shows the four-core accelerator gap voltage pulse under a beam load of 0.90 kA. The measured gap voltage of 195 kV is near the design value. Both core sets in the module were pulse

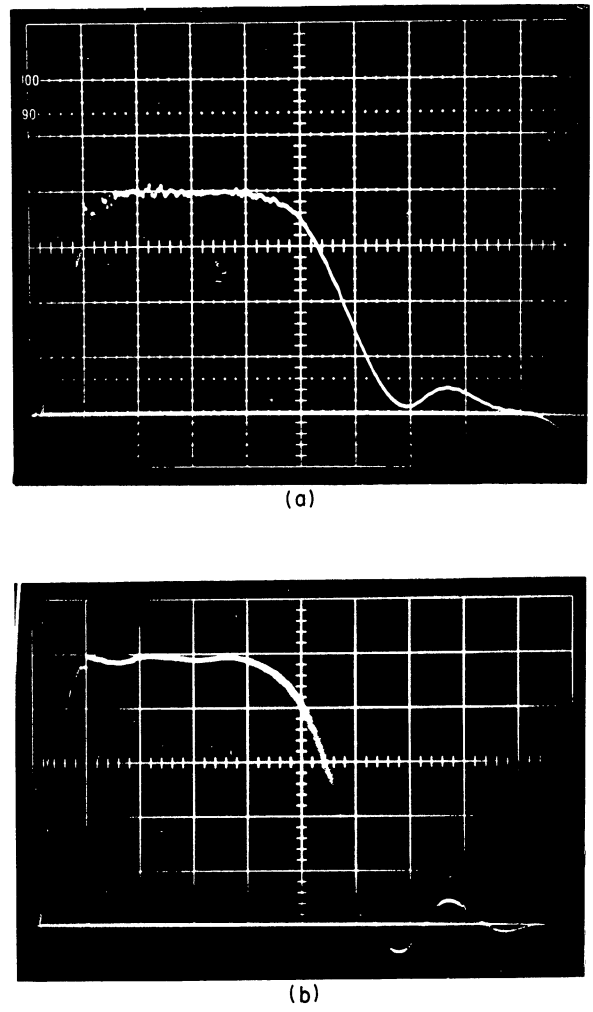

FIGURE 14 Oscilloscope trace of (a) injector voltage and (b) cathode current. Horizontal scale: 0.5 μsec/large division. Vertical scale: (a) 110 kV/large division, (b) 200 A/large division.

tested with beam near the design gap voltage of 200 kV. By adding the measured voltage pulses from the injector, four-core and five-core gaps during these tests, it was calculated that a peak output beam energy of 820 keV was achieved. Under these conditions, the total energy in the beam pulse is over 1.2 kJ and the peak beam power is over 700 MW. However, high-voltage breakdowns in the present accelerator gaps have limited any extensive operation to between 150 kV and 175 kV per gap, due to shortcomings in the present gap-electrode design. Therefore,

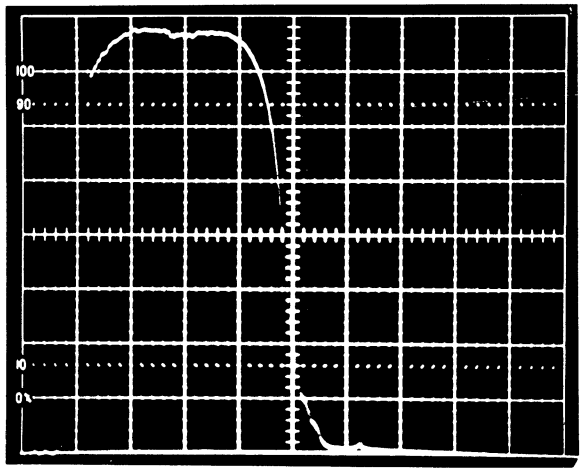

FIGURE 15 Oscilloscope trace of the electron beam current pulse at the accelerator exit. Horizontal scale: 0.5 μsec/large division. Vertical scale: 100 A/large division.

under more typical operation the prototype accelerator produces a beam of about 750 keV. This beam energy has been verified to within 5% by magnetic-deflection measurements.

In order to obtain an estimate of the beam energy spread, the voltage waveforms have been summed point-by-point in time and weighted by the corresponding transmitted current. The results, taken from the high-energy test data and shown in Fig. 17, indicate an energy spread of less than 3% (FWHM). This spread could be reduced by more careful tuning of the compensators. The energy spread in an accelerator composed of many accelerating modules would be reduced further by the random cancellation of the effects of slight irregularities in the waveforms produced by individual modulators.

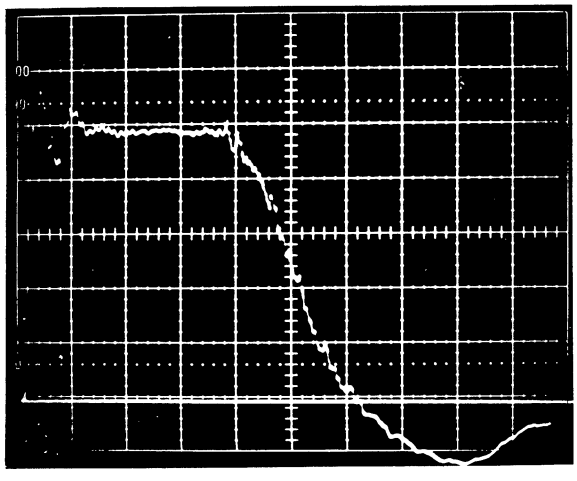

FIGURE 16 Oscilloscope trace of the four-core accelerator gap voltage pulse with a 900 A beam load. Horizontal scale: 0.5 μsec/large division. Vertical scale: 39 kV/large division.

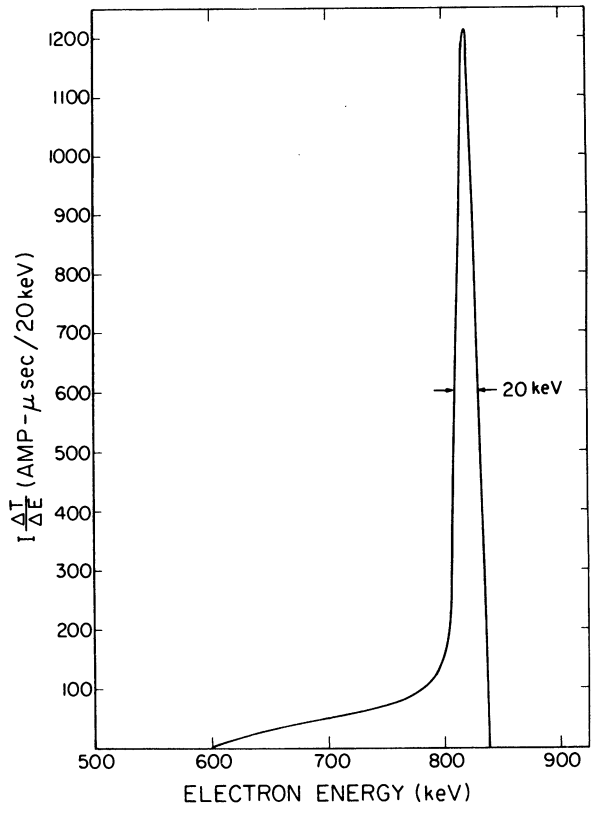

FIGURE 17 Computed energy distribution of the accelerated beam with the accelerator gaps operating near the design voltage.

The smallest beam spot thus far attained by the prototype induction accelerator is demonstrated in Fig. 18, which is an X-ray image of the electron beam focused onto a carbon plate 25 cm beyond the last solenoid at the exit of the accelerator (Fig. 12). If the 3-mm diameter aperture of the pinhole X-ray camera is taken into account, most of the beam appears focused into a diameter of less than 6 mm. In practice the beam is usually focused to a larger diameter to limit collector damage and to conduct stable beam-propagation studies.

In a high-energy design, it is important to maximize the energy per unit length. Since the pro-

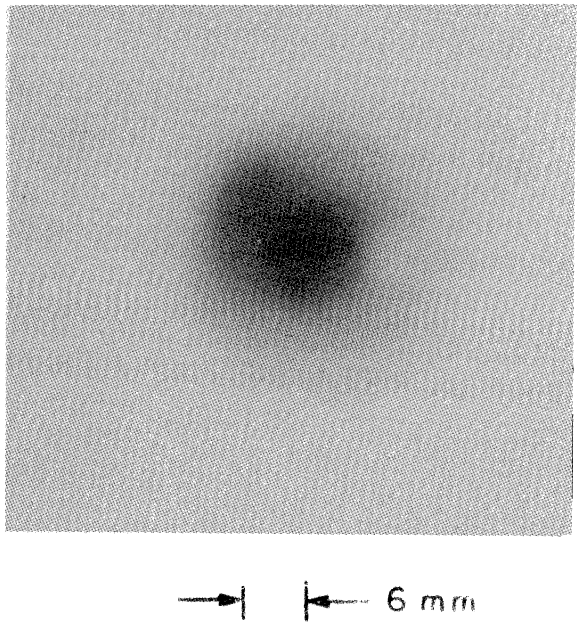

FIGURE 18 X-ray pinhole photograph of the accelerated electron beam spot incident on a carbon plate 25 cm beyond the last focus coil at the exit of the prototype accelerator.

totype module was constructed to accommodate design changes, there is more room around components than necessary. Without any significant modification of component dimensions, production modules could easily be made short enough to support a voltage gradient greater than 0.25 MeV per meter with a 2.0-μsec pulse length.

The prototype linear induction accelerator has been developed as a guide to the technology of a long-pulse, high-current, high-energy charged-particle accelerator. Many parameters remain to be optimized, depending on design goals. For example, in the course of further design studies, the accelerator ultimately resulting from these initial studies may achieve considerably higher volt-seconds per unit accelerator length.

5. CONCLUSION

A prototype module of a long-pulse, high-current linear induction accelerator has been designed, built and tested. Several innovations have been incorporated into its construction that demonstrate both the advantages and the technical feasibility of the efficient use of low-cost magnetic materials in a design aimed at minimum complexity of operation and high reliability at high energy gain per module. This demonstration module has been shown to be capable of driving over 2 kA at a voltage of 400 kV, which is kept constant for nearly 2 μsec.

In combination with a high-current electron injector, the prototype module becomes an accelerator that presently delivers a 2-μsec (FWHM) electron beam pulse at a current of 750 A and an energy of 750 keV. This system has been in operation for four years for the purpose of studying high-current beam transport with applications to advanced accelerator concepts.

REFERENCES

1. R. Avery, et al., *IEEE Trans. Nucl. Sci.* **NS-18,** 479 (1971).
2. J. W. Beal, N. C. Christofilos, and R. E. Hester, *IEEE Trans. Nucl. Sci.* **NS-16,** 294 (1969).
3. S. Penner, and A. Galejs, Beam Dynamics Studies, Internal Report, NBS, September 1972.
4. Resonance, Q Investigations and Beam Instability Studies of a High Current Induction Linac, Report No. HRC-703, February 1972. Prepared under contract no. NBS-1040-71 (Task 2) by Haimson Research Corp., N. W. Industrial Park, South Ave., Burlington, Massachusetts 01803.
5. R. W. Kuenning, Saturation Wave Analysis for Eddy Currents Entirely Within the Magnetic Strip, UCID 15029, September 19, 1966, and Eddy Current Analysis Extended for Times After the Inner Wrap Completely Saturates with Non-constant Applied Voltage, UCID 15031, September 23, 1966, Lawrence Radiation Laboratory, Livermore, California.
6. S. D. Winter, Magnetization of Tape Assuming Uniform Distribution of Nucleating Centers Throughout the Tape, UCID 15042, November 11, 1966, Lawrence Radiation Laboratory, Livermore, California.